Radar Forward-Looking Super-Resolution Imaging Algorithm of ITR-DTV Based on Renyi Entropy

Min Bao , *Member, IEEE*, Zhenhao Jia , *Student Member, IEEE*, Xiaoning Yin, *Student Member, IEEE*, and Mengdao Xing , *Fellow, IEEE*

Abstract—Radar forward-looking super-resolution imaging is a hot spot in the field of radar imaging research. Restricted by Doppler bandwidth and platform size, traditional high-resolution synthetic aperture imaging and real aperture imaging are not suitable for forward-looking imaging, so a deconvolution-based radar forward-looking super-resolution imaging technology is proposed. The traditional methods currently used in the field of forward-looking deconvolution super-resolution imaging of scanning radar have poor ability to recover the texture details of the target image direction, but simply describe the errors of all measurement data uniformly, which leads to an increase in the result error and have poor ability to adapt to different scenarios. So, this article proposes an improved Tikhonov regularization direction total variation (DTV) deconvolution super-resolution algorithm based on Rayleigh entropy. The algorithm introduces the DTV operator to more accurately restore the edge texture details of the image, and adds a weight matrix to the loss function to more accurately reflect the error degree of each measurement value in the loss function. The entropy enhances the applicability of the algorithm in different scenarios, and significantly improves the radar's ability to recover targets in a low signal-to-noise ratio environment. Finally, the simulation data and measured data processing results show that compared with the traditional method in the field of scanning radar forward looking deconvolution super-resolution imaging, the algorithm proposed in this article is better.

Index Terms—Direction total variation (DTV), forward-looking radar, Renyi entropy, super-resolution.

I. INTRODUCTION

RADAR forward-looking imaging technology is an important part of radar imaging, and it is urgently needed to improve the azimuth resolution of the radar's forward-looking area in practical engineering applications. Synthetic aperture technology can achieve high-resolution imaging in the side-looking and squint forward direction through the Doppler frequency changes caused by relative motion between the radar platform and targets [1]. However, the Doppler frequency change in radar forward imaging is basically zero, so synthetic aperture technology cannot be applied. To address this technical problem, domestic and foreign scholars have proposed solutions, such as real aperture scanning imaging technology, monopulse imaging technology, and forward-scanning deconvolution super-resolution imaging technology. However, despite the use of large-sized array antennas to improve resolution, the resolution of forward-looking imaging using real aperture radar still cannot meet practical application requirements [2]. The monopulse technique has high goniometric accuracy and can effectively improve the radar azimuth resolution. Compared with SAR and DBS, monopulse technology can realize imaging in the forward-looking area, but when adjacent targets are located in the same beam, monopulse technology cannot realize target resolution, resulting in the number of targets not being accurately estimated [3]. Conversely, the deconvolution operation provides a new technical means for radar forward-looking super-resolution imaging. By utilizing the super-resolution imaging technology of deconvolution, the azimuthal resolution enhancement problem can be converted into the inverse problem of deconvolution by reconstructing the azimuthal echo convolution model using a forward scanning time series containing target azimuth information [4]. Based on deconvolution-based super-resolution imaging technology, super-resolution can be achieved under low-cost and high-efficiency conditions without changing hardware. It can be made compatible with existing radar platforms by adding signal processing modules, which is conducive to the promotion and application of the technology.

Deconvolution techniques are highly sensitive to noise. To address its ill-posed problem, Richards [5] proposed an iterative noncorrelated super-resolution imaging method and a corresponding fast algorithm that can increase the angular resolution by about three times. However, this method has high requirements for scene SNR. In the 1990s, the nonlinear compensating filter super-resolution imaging method was proposed that improved angular resolution by 2-3 times. The generalized filtering method is also used to improve the imaging angular resolution by about four times [6]. However, due to the difficulty in accurately selecting the convergence parameters during the iterative process, the controllability of the convergence is poor, and the restored target azimuth signal will have angle deviation and poor noise suppression. In recent years, researchers have applied Bayesian statistical optimization methods in optical super-resolution to radar super-resolution imaging algorithms [7]. The

Min Bao, Zhenhao Jia, and Xiaoning Yin are with the School of Electronic Engineering, Xidian University, Xi'an 710071, China (e-mail: mbao@xidian.edu.cn; jiazhenhao2022@163.com).

Mengdao Xing is with the National Laboratory of Radar Signal Processing, Xidian University, Xi'an 710071, China.

relevant literature uses the maximum A posteriori criterion to estimate the target azimuth signal, and based on the statistical characteristics of the echo data, a Bayesian model is established to allow the azimuth information to quickly converge during the iterative process. However, when there is a large amount of noise in the receiver, the internal noise of the system will be amplified after deconvolution, resulting in ringing effects and large deviations between the reconstructed target azimuth signals and theoretical data. Due to this defect, researchers propose a regularization super-resolution method based on constrained optimization theory, which effectively alleviates the ill-posed problem in deconvolution [8].

The key to solving the deconvolution super-resolution problem with regularization methods lies in how to optimize the objective function to accurately and efficiently describe the target scene. Based on the L1 norm, the target azimuth signal can be reconstructed in sparse scenes with low SNR [9]. However, such methods are limited in their application scenario and have relatively high computational complexity. The iterative adaptive super-resolution imaging method gradually improves the pathology of the echo autocorrelation matrix through iterations with a robust super-resolution processing capability [10]. The improved TSVD algorithm is used to first preprocess the echo signal using the TSVD algorithm, and then adjust the truncation parameter k to remove the smaller singular values in the desired result and suppress the noise amplification [11]. The TV algorithm uses the total variation operator as the regularization term, and can effectively recover the contour feature information of the image [12]. However, using the TV algorithm is prone to the stair-step effect and the preservation of image texture components is not ideal. A regularization algorithm based on maximum entropy is also used in forward looking super-resolution imaging [13]. Since the influence of noise in the echo was not considered when verifying its performance, the performance of the algorithm under noisy environment is limited. Using maximum entropy as the regularization term can obtain the better reconstruction results when the target scene is relatively smooth [14]. When the target scene is sparse, choosing minimum entropy as the regularization factor can better reconstruct the target.

When there is numerous texture information in the actual scene and the interested target is distributed within a certain tilt angle range, the TV algorithm has isotropic properties that are disadvantageous for preserving directional textures. Therefore, in order to more accurately extract the target information and suppress the stair-step effect of the image, the algorithm proposed in this article first adds the directional total variation (DTV) operator as a regularization term. According to [15], using a single maximum or minimum entropy as a regularization term can only have better super-resolution effect in specific target scenes. Therefore, to enhance the algorithm's adaptability to different application scenarios, a Renyi entropy with an adjustable parameter is added as another regularization term. Finally, analyzing the error term in the traditional objective function, the same weight is applied to the error term, but in actual systems, each measurement value has different error levels. Therefore, in order to more accurately describe the error,
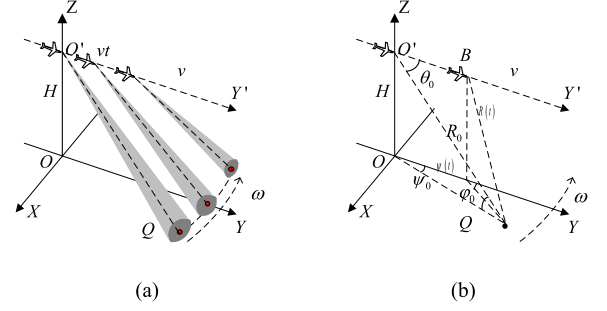

Fig. 1. Radar forward-looking model. (a) Radar scanning process. (b) Radar geometric model.

a weighted matrix $\mathbf{W}_1$ is introduced into the error term of the objective function. Thus, this article constructs a completely new optimization function to solve the target problem, in order to further preserve the directional textures and edge characteristics of the image, enhance the algorithm's adaptability to different scenes, and reduce the influence of error. The validity of the algorithm is verified through simulations and actual measured data.

II. RADAR FORWARD IMAGING ECHO MODEL

This article mainly studies the super-resolution problem of radar forward-looking imaging. In most cases, the radar platform is in motion, and the stationary state can be considered as a special type of motion state. Therefore, this article mainly focuses on the derivation and explanation of the motion geometric model of radar forward-looking imaging. Fig. 1 shows the geometric model of the motion platform scanning radar imaging. Fig. 1(a) shows the radar scanning process, where the distance between the carrier and the target plane is H, the platform moves along the Y-axis at a speed of v, and the radar beam scans at an angular velocity of ω. The geometric model of the relative position between the moving platform and the target is shown in Fig. 1(b), where the beam elevation angle is φ and the azimuth angle at the beginning of scanning is θ_0.

Assume that there is a target point P on the target plane and the target is always within the beam range. When $t = 0$, the aircraft is at the initial position O', the distance between the aircraft and P is R_0, and the angle between OP and the Y-axis is θ_0. When the aircraft moves along the Y-axis for time t, the instantaneous distance from the radar to point B is $\mathrm{R}(t)$, and the projection distance from the aircraft on the XOY plane to point P is r. Therefore, from the geometric relationship in Fig. 1(b), we can obtain that at time t, the approximate linear slant range expression obtained by Taylor series expansion of the distance between the aircraft and the target point P is

$$
\begin{aligned}
R(t) &= \sqrt{H^2 + r^2} \\
&= R_0 - vt \cos \theta_0 \\
&\quad + \frac{v^2 \sin^2 \theta_0}{2R_0} t^2 + \mathrm{O}(t) \\
&\approx R_0 - vt \cos \theta_0.
\end{aligned}
\tag{1}
$$

In practical application, R_0 is usually large due to the long radar action distance. And the antenna beam sweeps over the target for a very short time, resulting in a very small t. Together with $\sin\theta_0 \leq 1$, we can get $\frac{v^2\sin^2\theta_0}{2R_0}t^2 \ll vt\cos\theta_0$, thus the higher order terms in (1) can be approximately neglected. Radar emits linearly chirped signals at a certain pulse repetition frequency, and thus the transmission signal expression is

$$s(\tau) = \text{rect}\left(\frac{\tau}{T_r}\right)\cos\left\{2\pi f_0\tau + \pi K_r\tau^2\right\} \qquad (2)$$

where τ is the time in the range direction, T_r is the width of the transmitted signal pulse, f_0 and K_r are the frequency modulation rates of the carrier wave and linear frequency modulation signal.

For LFM signals, the carrier frequency portion is first removed using the dechirp technique. Then, pulse compression is performed, which is generally realized using matched filters. The original echo signal of the point target radar, after matched filtering in the frequency domain, is transformed back to the time domain in the frequency domain using IFFT. After the carrier frequency is removed from the echo signal at time t, and the time variable is replaced by a spatial variable, the expression for the echo in terms of azimuth angle θ and distance R is obtained

$$s(R,\theta) = \tilde{\sigma}(R,\theta) \otimes A(R,\theta)\exp\left\{j\frac{4\pi f_0}{c}v\cos\varphi\frac{\theta - \theta_a}{\omega}\right\} \qquad (3)$$

where $\otimes$ represents convolution operation, and $A(R,\theta) = h(\theta)\sin c(\frac{2B}{c}R)$ represents the impulse response function. For a typical radar forward-looking scanning imaging system, range migration correction can be used to eliminate the effects of platform motion. Range migration correction function is $H(f_\tau,\tau) = \exp(j2\pi f_\tau\frac{v\tau}{c})$. After the range migration correction, the echo signal can be represented as the convolution of the antenna pattern and the target scattering information. The Doppler shift $\exp[-j2\pi f_0\tau_d]$ can be further written as $\exp[-j\frac{4\pi}{\lambda}(R_0 - vt\cos\theta_0\cos\beta)]$. Therefore, when the radar platform is moving at a low speed, the Doppler shift in any direction in the forward-looking region $[-10\circ, 10\circ]$ is almost the same, which is negligible in practical applications. The Doppler phase measurement matrix is also introduced to reduce the error between the echo model and the echo data.

As can be seen from the above equation, the pre-processed echo signal in the azimuth direction can be expressed in the form of the antenna radiation pattern convolved with the target scattering coefficient. Taking into account the existence of noise and the fact that the echo received by the radar is a discrete point, the echo signal is re-expressed in a 1-D convolution form

$$s(t) = a(t) \otimes \sigma + n(t) \qquad (4)$$

where $a(t)$ represents the convolution matrix composed of the antenna radiation pattern, and $n(t)$ represents the random noise in the imaging process. It can be seen from (4) that solving the super-resolution problem of radar forward-looking imaging is equivalent to solving the estimation problem of the target scattering coefficient σ.

III. ITR-DTV REGULARIZATION ALGORITHM BASED ON RENYI ENTROPY

According to the geometric model of radar forward scanning imaging derived in the previous section, it can be seen that in practical engineering applications, noise inevitably exists in the system. Therefore, the data information cannot be directly restored by the deconvolution algorithm, and the signal will be submerged in strong noise. In addition, the non-rank characteristics of the antenna radiation pattern make it such that even a small disturbance in the system can cause a large error in the final restored result. Therefore, it is very important to select a suitable regularization term to form the objective function for analyzing and solving the ill-posed deconvolution problem.

The objective function constructed using regularization method is [16]

$$\arg\min_{\sigma}\|A\sigma - s\|_2^2 + \lambda\|\Gamma(\sigma)\|_q^q \qquad (5)$$

where q denotes a norm operation, λ denotes the regularization parameter, and $\Gamma(\sigma)$ denotes a function with respect to σ.

Total variation regularization is a representative algorithm in regularization methods. It has been widely used in achieving super-resolution with good results in image convolution inversion. However, the traditional total variation function has rotation invariance, that is, after any rotational transformation, the total variation function values in all directions of the image are the same. Therefore, on the basis of traditional total variation regularization algorithm, the DTV algorithm was proposed [17], which keeps and restores the contour and texture details of the image better, resulting in better target reconstruction performance. The definition of the DTV regularization term is

$$\text{DTV}(f) = \sum_{i,j}\sup_{t \in E_{\alpha,\theta}}\langle\Delta f(i,j),t\rangle \qquad (6)$$

where $\alpha > 1, \theta \in [-\frac{\pi}{2}, \frac{\pi}{2}]$.

The region enclosed by an ellipse with a major axis of length α, a minor axis of length 1, and an angle of inclination of θ is expressed as $E_{\alpha,\theta}$. If the set of all vectors within a unit circle is represented as B_2, then $E_{\alpha,\theta}$ can be seen as the result of stretching and rotating B_2. Therefore, the relationship between $E_{\alpha,\theta}$ and B_2 can be expressed as

$$\mathbf{E}_{\alpha,\theta} = \mathbf{R}_\theta\mathbf{\Lambda}_\alpha\mathbf{B} \qquad (7)$$

where $\mathbf{R}_\theta = \begin{bmatrix}\cos\theta & -\sin\theta \\ \sin\theta & \cos\theta\end{bmatrix}$, $\mathbf{\Lambda}_\alpha = \begin{bmatrix}\alpha & 0 \\ 0 & 1\end{bmatrix}$, the (6) can also be expressed as

$$\text{DTV}(f) = \sum_{i,j}\sup_{t \in E_{\alpha,\theta}}\langle\Delta f(i,j),t\rangle$$
$$= \sum_{i,j}\|\mathbf{\Lambda}_\alpha\mathbf{R}_\theta\Delta f(i,j)\|_2. \qquad (8)$$

From (8), it can be determined that the weights of the gradients used in the direction total variation regularization method for super-resolution imaging depend on their respective directions. Therefore, in order to increase the sensitivity of the algorithm

to changes in the selected direction, better suppress the stair-stepping effect, and better maintain the texture and edge characteristics of the image, the direction total variation operator is selected as the regularization term in this article instead of the total variation operator.

In practical radar systems, the radar receiver is not in an ideal state. Due to the combined effects of the internal equipment of the receiver and the external environment, each measurement value in the radar system has a different degree of error. By adding a weighting matrix to the loss function terms, the system can evaluate measurements more accurately, thus improving the performance and reliability of the radar system. A weighting matrix is defined to more accurately characterize the errors in each measurement and assign different weights to them depending on their different magnitudes. Therefore, $|\mathbf{e}_j|^p$ is utilized to assign different weights and the weighting matrix is constructed as

$$\mathbf{W}_1 = diag\left(|\mathbf{e}_1|^p + \eta, \cdots, |\mathbf{e}_m|^p + \eta\right) \qquad (9)$$

where $\mathbf{e}_j = \mathbf{s}_j - \mathbf{A}_j \boldsymbol{\sigma}_0$, $\mathbf{A}_j$ is the jth row of matrix $\mathbf{A}$. s_j is the jth element of $\mathbf{s}$ and $\boldsymbol{\sigma}_0$ is an initial matrix value of $\boldsymbol{\sigma}$, $p \geq 0, \eta \geq 0$.

Based on the above analysis, this article adds a weight matrix $\mathbf{W}_1$ to the algorithm's error term $||\mathbf{s} - \mathbf{A}\sigma||^2$, while using the direction total variation operator as the regularization term to maintain the texture and edge characteristics of the image. By adjusting the direction vectors in the direction total variation operator, better super-resolution effects can be achieved for the main texture directions in the image, and the appearance of the stair-stepping effect can be suppressed to some extent. The optimized model can be expressed as

$$J(\boldsymbol{\sigma}) = ||\boldsymbol{W}_1^{-1}\left(\boldsymbol{s} - \boldsymbol{A}\boldsymbol{\sigma}\right)||^2 + \mathrm{DTV}\left(\boldsymbol{\sigma}\right)$$
$$= ||W_1^{-1}\left(\boldsymbol{s} - \boldsymbol{A}\boldsymbol{\sigma}\right)||^2 + \sum_i \|\boldsymbol{P}_i \Delta \boldsymbol{\sigma}_i\|_2^2 \qquad (10)$$

where $\boldsymbol{P}_i \Delta \boldsymbol{\sigma}_i$ can be expressed as

$$\boldsymbol{P}_i \Delta \boldsymbol{\sigma}_i = \Delta \boldsymbol{\sigma}_i - \langle \xi_i, \Delta \boldsymbol{\sigma}_i \rangle \xi_i \qquad (11)$$

where $\langle \cdot, \cdot \rangle$ represents the inner product of vectors, Δ represents the total variation operator, $\xi \in U^2$, $\|\xi_i\| \leq \gamma < 1$ is a vector that determines the direction, $\boldsymbol{P} \in U^{2 \times 2}$, $\boldsymbol{P}_i = \boldsymbol{I} - \xi_i \otimes \xi_i$ is a weighted matrix, and $\otimes$ represents the outer product of vectors.

The total variation operator Δ can be represented in matrix form as follows [18]:

$$\Delta = \boldsymbol{D} = \begin{bmatrix} \boldsymbol{D}_x \\ \boldsymbol{D}_y \end{bmatrix} \qquad (12)$$

where
$$\boldsymbol{D}_x = \begin{bmatrix} -\boldsymbol{I} & \boldsymbol{I} & & \\ & \ddots & \ddots & \\ & & -\boldsymbol{I} & \boldsymbol{I} \end{bmatrix}, \qquad \boldsymbol{D}_y =$$

$$\begin{bmatrix} \boldsymbol{D}_1 & & & \\ & \boldsymbol{D}_1 & & \\ & & \ddots & \\ & & & \boldsymbol{D}_1 \end{bmatrix}, \qquad \boldsymbol{D}_1 = \begin{bmatrix} -1 & 1 & & \\ & \ddots & \ddots & \\ & & -1 & 1 \end{bmatrix}, \qquad \text{the}$$

dimension of the matrix operator is $n_x(n_y - 1) \times n_x n_y$. $\boldsymbol{I}$ represents a unit vector of length n_x.

Therefore, the optimization model can be expressed as

$$J(\boldsymbol{\sigma}) = ||\boldsymbol{W}_1^{-1}\left(\boldsymbol{s} - \boldsymbol{A}\boldsymbol{\sigma}\right)||^{\mathbf{2}} + \mathrm{DTV}\left(\boldsymbol{\sigma}\right)$$
$$= ||\boldsymbol{W}_1^{-1}\left(\boldsymbol{s} - \boldsymbol{A}\boldsymbol{\sigma}\right)||^{\mathbf{2}} + \|\boldsymbol{PD}\boldsymbol{\sigma}\|_{\mathbf{2}}^{\mathbf{2}}. \qquad (13)$$

In practical situations, the echo data obtained by the radar through forward scanning is complex. Therefore, the echo data can be expressed in the form of amplitude and phase separation, and the target scattering matrix is

$$\boldsymbol{\sigma} = \boldsymbol{\phi}\boldsymbol{f} \qquad (14)$$

where $\boldsymbol{\phi} = diag\{\exp[j\varphi(\boldsymbol{\sigma})]\}$ is a diagonal matrix, $\varphi(\boldsymbol{\sigma})$ is the phase of $\boldsymbol{\sigma}$, and $\boldsymbol{f}$ is the amplitude $|\boldsymbol{\sigma}|$ of $\boldsymbol{\sigma}$. Eq. (14) shows that parameters related to amplitude and phase can be separated, which is convenient for solving the objective function with the ADMM algorithm in the subsequent steps. The observation model is reshaped as $s = A\boldsymbol{\phi}\boldsymbol{f} + \boldsymbol{n}$, and the optimization problem of adding the total variation term in a certain direction can also be re-expressed as follows:

$$\min \|\boldsymbol{PD}\boldsymbol{f}\|_2^2 \, s.t. \, \|\boldsymbol{s} - \boldsymbol{A}\boldsymbol{\phi}\boldsymbol{f}\|_2^2 \leq \varepsilon \qquad (15)$$

where the $\|\boldsymbol{PD}\boldsymbol{f}\|_2^2$ is a nondifferentiable term. Therefore, variable separation and penalty optimization methods [19] are considered. By introducing variable $\boldsymbol{\omega}$ to replace $\mathrm{P}\Delta\boldsymbol{\sigma}$ and constraining the residual terms of $\boldsymbol{\omega}$ and $\mathrm{P}\Delta\boldsymbol{\sigma}$, the optimization model can be expressed as

$$J(\boldsymbol{f}) = ||\boldsymbol{W}_1^{-1}\left(\boldsymbol{s} - \boldsymbol{A}\boldsymbol{\phi}\boldsymbol{f}\right)||^2 + \|\boldsymbol{\omega}\|_2^2 + \frac{\beta_1}{2}\|\boldsymbol{PD}\boldsymbol{f} - \boldsymbol{\omega}\|_2^2 \qquad (16)$$

where β_1 represents the regularization parameter.

In information theory, Renyi entropy has an important diversity indicator, which is an extension of Shannon entropy. Renyi entropy contains a variable parameter α, and the Renyi entropy of order α is defined as

$$R_\alpha(X) = \frac{1}{1-\alpha}\ln\left(\sum_{i=1}^n P_i^\alpha\right) \qquad (17)$$

where X represents the set of all samples, $\alpha \geq 0$ and $\alpha \neq 1$, P_i represents the probability of the ith variable appearing, $P_i > 0$ and $\sum_{i=1}^n P_i = 1$.

1) When $\alpha = 0$, the probability of each event in the set X appearing is equal and the entropy value is the highest. The expression is

$$R_0(X) = \ln n. \qquad (18)$$

2) When $\alpha \to 1$, $R_0(X)$ degenerates into Shannon entropy with expression

$$\lim_{\alpha \to 1} R_\alpha(X) = \lim_{\alpha \to 1} \frac{1}{1-\alpha}\ln\left(\sum_{i=1}^n P_i^\alpha\right)$$
$$= -\sum_{i=0}^n P_i \ln(P_i). \qquad (19)$$

3) When $\alpha \to \infty$, $R_\alpha(X)$ converges to the minimum entropy with expression

$$R_\infty(X) = -\ln P_i^{\max} \qquad (20)$$

where $P_i^{\max}$ represents the probability of the event with the highest probability in set X.

The above definition of Renyi entropy shows that it contains a variable parameter α that can be set to different values according to different scenarios, so that Renyi entropy can more accurately represent the characteristics of the current target scenario. Therefore, to maximize the use of target prior information, reduce sensitivity to noise interference, and enhance the applicability of the algorithm to different scenarios, Renyi entropy is selected as another regularization term to constrain the target amplitude, resulting in the final optimized model as

$$J(\boldsymbol{f}) = ||\boldsymbol{W}_1^{-1}(\boldsymbol{s}-\boldsymbol{A}\boldsymbol{\phi}\boldsymbol{f})||^2 + ||\boldsymbol{\omega}||_2^2 + \frac{\beta_1}{2}||\boldsymbol{PD}\boldsymbol{f}-\boldsymbol{\omega}||_2^2$$
$$+ \boldsymbol{\lambda_1}\exp\left(\frac{1}{1-\boldsymbol{\alpha}}\ln\boldsymbol{f}^{\boldsymbol{\alpha}}\right). \quad (21)$$

Using the ADMM method to iteratively solve the above model, we construct the corresponding augmented Lagrange function, and obtain the solution model function as follows:

$$J(\boldsymbol{f}) = ||\boldsymbol{W}_1^{-1}(\boldsymbol{s}-\boldsymbol{A}\boldsymbol{\phi}\boldsymbol{f})||^2 + ||\boldsymbol{\omega}||_2^2 - \boldsymbol{\lambda}^T(\boldsymbol{PD}\boldsymbol{f}-\boldsymbol{\omega})$$
$$+ \frac{\boldsymbol{\beta_1}}{2}||\boldsymbol{PD}\boldsymbol{f}-\boldsymbol{\omega}||_2^2 + \lambda_1\exp\left(\frac{1}{1-\boldsymbol{\alpha}}\ln\boldsymbol{f}^{\boldsymbol{\alpha}}\right) \quad (22)$$

where λ is the Lagrange multiplier.

During the solving process, it is necessary to iteratively update variable $\boldsymbol{\omega}$, $\boldsymbol{f}$ and $\boldsymbol{\phi}$. As their updates do not affect each other, the method of separating variables is used to transform it into a sub-problem about $\boldsymbol{\omega}$, $\boldsymbol{f}$ and $\boldsymbol{\phi}$ for solving.

Concerning the subproblem of $\boldsymbol{\omega}$

$$\boldsymbol{\omega}^{(n+1)} = \arg\min\left\|\boldsymbol{\omega}^{(n)}\right\|_2^2 + \frac{\beta_1}{2}\left\|\boldsymbol{PD}\boldsymbol{f}-\boldsymbol{\omega}^{(n)}\right\|_2^2$$
$$- \boldsymbol{\lambda}^T\left(\boldsymbol{PD}\boldsymbol{f}-\boldsymbol{\omega}^{(n)}\right). \quad (23)$$

To solve the problem, the standard contraction formula is used. The isotropic contraction operator $shrink_2$ is defined as

$$\text{shrink}_2(b,\mu) = \begin{cases} 0, & b=0 \\ (\|b\|_2-\mu)\frac{b}{\|b\|_2}, & b\neq 0. \end{cases} \quad (24)$$

Therefore, the closed-form solution of (23) can be expressed as

$$\boldsymbol{\omega}^{(n+1)} = \max\left\{\left\|\boldsymbol{PD}\boldsymbol{f}-\frac{\boldsymbol{\lambda}}{\beta_1}\right\|_2 - \frac{1}{\beta_1}, 0\right\}\frac{\boldsymbol{PD}\boldsymbol{f}-\frac{\boldsymbol{\lambda}}{\beta_1}}{\left\|\boldsymbol{PD}\boldsymbol{f}-\frac{\boldsymbol{\lambda}}{\beta_1}\right\|_2}. \quad (25)$$

Concerning the subproblem of $\boldsymbol{f}$

$$\boldsymbol{f}^{(n+1)} = \arg\min\left\|\boldsymbol{W}_1^{-1}\left(\boldsymbol{s}-\boldsymbol{A}\boldsymbol{\phi}\boldsymbol{f}^{(n)}\right)\right\|^2$$
$$- \boldsymbol{\lambda}^T\left(\boldsymbol{PD}\boldsymbol{f}^{(n)}-\boldsymbol{\omega}\right)$$
$$+ \frac{\beta_1}{2}\left\|\boldsymbol{PD}\boldsymbol{f}^{(n)}-\boldsymbol{\omega}\right\|_2^2$$
$$+ \lambda_1\left(\frac{1}{1-\alpha}\ln\left(\boldsymbol{f}^{(n)}\right)^{\alpha}\right). \quad (26)$$

To solve the minimization problem shown in (26), we need to take the derivative of A to find its stationary point

$$\nabla\boldsymbol{f} = 2\boldsymbol{\phi}^H\boldsymbol{A}^H\boldsymbol{W}_{11}\boldsymbol{A}\boldsymbol{\phi}\boldsymbol{f} - 2\boldsymbol{\phi}^H\boldsymbol{A}^H\boldsymbol{W}_{11}\boldsymbol{s} - \boldsymbol{D}^H\boldsymbol{P}^H\boldsymbol{\lambda}$$
$$+ \beta_1\boldsymbol{D}^H\boldsymbol{P}^H(\boldsymbol{PD}\boldsymbol{f}-\boldsymbol{\omega}) + \lambda_1\left(\frac{\alpha}{1-\alpha}\boldsymbol{f}^{\frac{2\alpha-1}{1-\alpha}}\right). \quad (27)$$

Further splitting the combined term containing $\boldsymbol{f}$ yields

$$\nabla\boldsymbol{f} = H(\boldsymbol{f})\boldsymbol{f} - \boldsymbol{D}^H\boldsymbol{P}^H\boldsymbol{\lambda} - \beta_1\boldsymbol{D}^H\boldsymbol{P}^H\boldsymbol{\omega} \quad (28)$$

where $\begin{aligned}H(\boldsymbol{f}) = &2\boldsymbol{\phi}^H\boldsymbol{A}^H\boldsymbol{W}_{11}\boldsymbol{A}\boldsymbol{\phi} + \beta_1\boldsymbol{P}^H\boldsymbol{D}^H\boldsymbol{D}\boldsymbol{P}\\&-2\boldsymbol{\phi}^H\boldsymbol{A}^H\boldsymbol{W}_{11}\boldsymbol{s}\boldsymbol{\phi} + \frac{\alpha\lambda_1}{1-\alpha}\boldsymbol{\phi}\boldsymbol{G}\end{aligned}$, $\boldsymbol{G} = diag\{g_1,\cdots,g_n\}$, and $g_i = |\sigma_i|^{\frac{3\alpha-2}{1-\alpha}}$.

Set $\nabla\boldsymbol{f} = 0$ in (28), the update formula for B can be expressed as

$$\boldsymbol{f}^{(n+1)} = H\left(\boldsymbol{f}^{(n)}\right)^{-1}\left(\boldsymbol{P}^H\boldsymbol{D}^H\boldsymbol{\lambda} + \beta_1\boldsymbol{P}^H\boldsymbol{D}^H\boldsymbol{\omega}\right). \quad (29)$$

Concerning the subproblem of $\boldsymbol{\phi}$

Use $\boldsymbol{\alpha}$ to represent the column vector composed of the diagonal elements of the phase diagonal matrix $\boldsymbol{\phi}$, and use $\mathbf{K}$ to represent the diagonal matrix $diag(f)$ with the amplitude as its diagonal elements. The solution of subproblem $\boldsymbol{\phi}$ is transformed into the solution of subproblem $\boldsymbol{\alpha}$

$$\boldsymbol{\alpha}^{(n+1)} = \arg\min\boldsymbol{s}^H\boldsymbol{W}_{11}\boldsymbol{s}$$
$$+ \left(\boldsymbol{\alpha}^{(n)}\right)^H\mathbf{K}^H\boldsymbol{A}^H\boldsymbol{W}_{11}\boldsymbol{A}\mathbf{K}\boldsymbol{\alpha}^{(n)}.$$
$$- \boldsymbol{s}^H\boldsymbol{W}_{11}\boldsymbol{A}\mathbf{K}\boldsymbol{\alpha}^{(n)} - \left(\boldsymbol{\alpha}^{(n)}\right)^H\mathbf{K}^H\boldsymbol{A}^H\boldsymbol{W}_{11}\boldsymbol{s} \quad (30)$$

Use the quasi-Newton methods to solve (30), its derivative is

$$\nabla\boldsymbol{\alpha} = 2\mathbf{K}^H\boldsymbol{A}^H\boldsymbol{W}_{11}\boldsymbol{A}\mathbf{K}\boldsymbol{\alpha} - 2\mathbf{K}^H\boldsymbol{A}^H\boldsymbol{W}_{11}\boldsymbol{s}. \quad (31)$$

Simplify (31), we obtain

$$\nabla\boldsymbol{\alpha} = H(\boldsymbol{\alpha})\boldsymbol{\alpha} - 2\mathbf{K}^H\boldsymbol{A}^H\boldsymbol{W}_{11}\boldsymbol{s} \quad (32)$$

where $H(\boldsymbol{\alpha}) = 2\mathbf{K}^H\boldsymbol{A}^H\boldsymbol{W}_{11}\boldsymbol{A}\mathbf{K}$.

The iterative update formula for A is

$$\boldsymbol{\alpha}^{(n+1)} = \boldsymbol{\alpha}^{(n)} - \gamma\left[H\left(\boldsymbol{\alpha}^{(n)}\right)\right]^{-1}\nabla\boldsymbol{\alpha}^{(n)} \quad (33)$$

where γ is the iteration step size.

Finally, since the problem being solved is a convex optimization problem and the variables $\boldsymbol{\omega},\boldsymbol{f}$, and $\boldsymbol{\phi}$ are solved independently of each other, the solution of λ^{n+1} is known to converge according to the ADMM algorithm. In practice, it usually converges around 30 iterations. The update of the Lagrange multiplier $\boldsymbol{\lambda}$ can be expressed as

$$\boldsymbol{\lambda}^{n+1} = \boldsymbol{\lambda}^n + \beta_1(\boldsymbol{\omega}-\boldsymbol{PD}\boldsymbol{f}). \quad (34)$$

Based on the above derivation and analysis, the solution process is listed as follows for easier reading listed in Table I.

TABLE I
STEPS FOR SOLVING ITR-DTV REGULARIZATION ALGORITHM BASED ON
RENYI ENTROPY USING ADMM METHOD

Input: Radar echo signal S, convolution matrix A,
maximum number of iterations MaxIter, and iteration
threshold ε

1. Given parameters: $p, \eta, \beta_1, \lambda_1, \alpha$;

2. Given initial vector: $\sigma^{(0)}, \omega^{(0)}, \lambda^{(0)}, \xi, f^{(0)}$;

3. $n = 0, 1, 2, L$, Perform the following steps:

(1) Update the Lagrange multiplier λ^{n+1} according to
Equation $\lambda^{n+1} = \lambda^n + \beta_1 (\omega - PDf)$;

(2) Update the slack variable $\omega^{(n+1)}$ according to Equation

$$\omega^{(n+1)} = \max \left\{ \left\| PDf - \frac{\lambda}{\beta_1} \right\|_2 - \frac{1}{\beta_1}, 0 \right\} \frac{PDf - \frac{\lambda}{\beta_1}}{\left\| PDf - \frac{\lambda}{\beta_1} \right\|_2};$$

(3) Update the target amplitude $f^{(n+1)}$ according to
Equation $f^{(n+1)} = H(f^{(n)})^{-1}(P^H D^H \lambda + \beta_1 P^H D^H \omega)$,

where $H(f) = 2\phi^H A^H W_{11} A\phi + \beta_1 P^H D^H DP - 2\phi^H A^H W_{11} s\phi + \frac{\alpha\lambda_1}{1-\alpha}\phi G$,

$G = diag\{g_1, L, g_n\}$, $g_i = |\sigma_i|^{\frac{3\alpha-2}{1-\alpha}}$;

(4) Update the phase $\alpha^{(n+1)}$ according to Equation
$\alpha^{(n+1)} = \alpha^{(n)} - \gamma \left[H(\alpha^{(n)}) \right]^{-1} \nabla\alpha^{(n)}$,

where $H(\alpha) = 2K^H A^H W_{11} AK$, K represents the diagonal
matrix $diag(f)$ with amplitude as the diagonal element.

(5) If $\frac{\left\| f^{(n+1)} - f^{(n)} \right\|_2}{\left\| f^{(n)} \right\|_2} < \varepsilon$ or the maximum number of iterations

n = Maxiter is reached, terminate the loop and output
$f^{(n+1)}$; else, go to step (1).

Output: the information of target scattering coefficient,
$f^{(n+1)}$ and $\alpha^{(n+1)}$.

TABLE II
PARAMETER SETTINGS FOR FORWARD IMAGING SIMULATION

parameters	values
Antenna beam width	$3\pi/180$ rad
antenna scan speed	$30\pi/180$ rad/s
transmitted signal carrier frequency	16 GHz
transmitted signal bandwidth	5 MHz
antenna scan range	$-4° \sim 4°$
target range	5Km

IV. SIMULATION EXPERIMENT AND ACTUAL MEASUREMENT DATA ANALYSIS

A. Experimental Design

The parameters for the radar forward imaging are set as
follows set in Table II.

For the point target simulation experiment, five points loca-
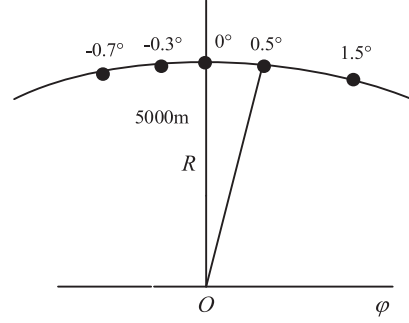tions located at the same distance but different azimuths, and

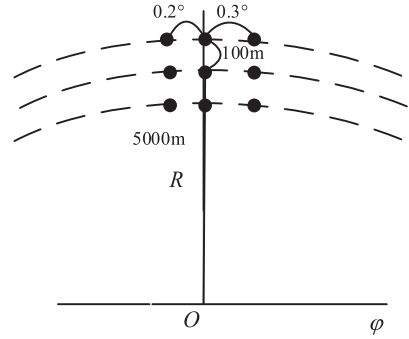Fig. 2. Distribution of point targets under the same distance condition.

Fig. 3. Distribution of 2-D array targets under different distance conditions.

the azimuth positions of the five points were defined as $-0.7°$,
$-0.3°$, $0°$, $0.5°$, and $1.5°$, as shown in Fig. 2.

For the simulation experiment of array targets, nine points lo-
cated at different distances and different azimuths were selected
as shown in Fig. 3.

Under the same signal-to-noise ratio, compare the imaging
results of the algorithm proposed in this article with other
algorithms to intuitively evaluate the performance of the new
algorithm. In addition, the relative imaging error can be used to
quantitatively describe the effectiveness of the super-resolution
algorithm. The relative error formula can be expressed as

$$\text{RIE} = \frac{\|\hat{\sigma} - \sigma\|_2}{\|\sigma\|_2} \tag{35}$$

where $\hat{\sigma}$ represents the recovered scattering information, and σ
represents the actual scattering information.

B. Simulation Experiment

For the ground background, assuming that noise follows
a Gaussian distribution, Fig. 4 shows the imaging results of
different methods under a signal-to-noise ratio of 15 dB.

From Fig. 4, it can be seen that the IAA super-resolution
result completely submerges the target in noise, and cannot
achieve the resolution of point targets in different azimuths. The
TSVD-L1 algorithm can roughly distinguish the positions of the
five point targets, but the average noise amplitude is large and
two false targets with relatively high energy appear, resulting
in significant amplitude loss of the actual target. The TV-L1
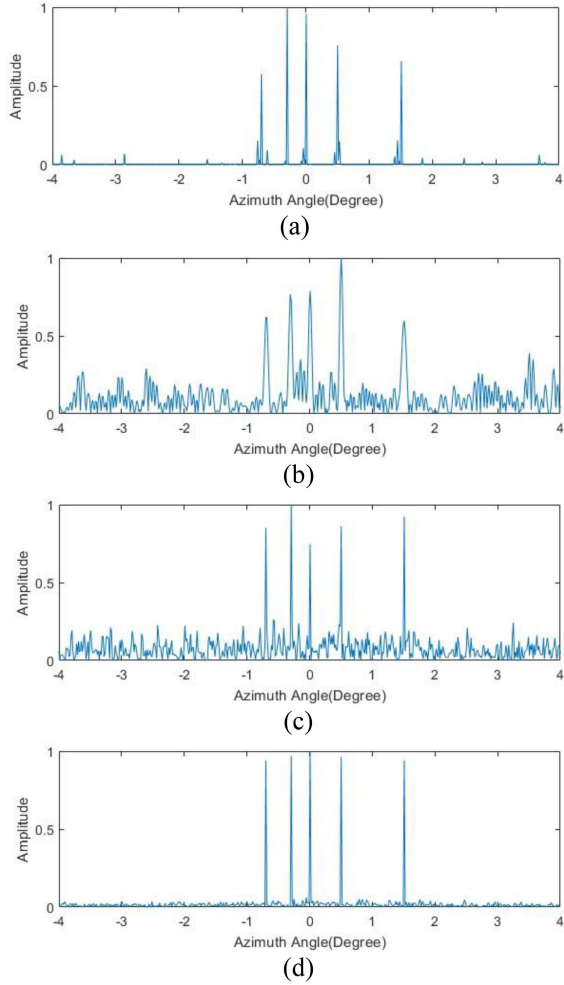algorithm achieves very good super-resolution for azimuthal

Fig. 4.   Comparison of one1-D point target super-resolution results. (a) IAA. (b) TSVD-L1. (c) TV-L1. (d) Proposed algorithm.

TABLE III
COMPARISON OF QUANTITATIVE ANALYSES OF SIMULATIONS

Method	real computation time
IAA	78.32s
TSVD-L1	70.68s
TV-L1	42.93s
The proposed algorithm	27.74s

targets, separating all point targets, but some higher amplitude noise points still remain, and the amplitude of the target signals also suffers some loss. When the proposed algorithm is used for recovery, most of the energy is concentrated on the target points, and there are no false targets, effectively suppressing the noise and achieving super-resolution recovery of the target. To quantitatively evaluate the proposed algorithm, we compare it with the remaining three algorithms in terms of real computation time. As given in Table III, the proposed algorithm has a lighter computational burden and faster convergence with the same super-resolution performance.

Fig. 5 shows that under the influence of noise, the target information in the IAA super-resolution result is almost submerged
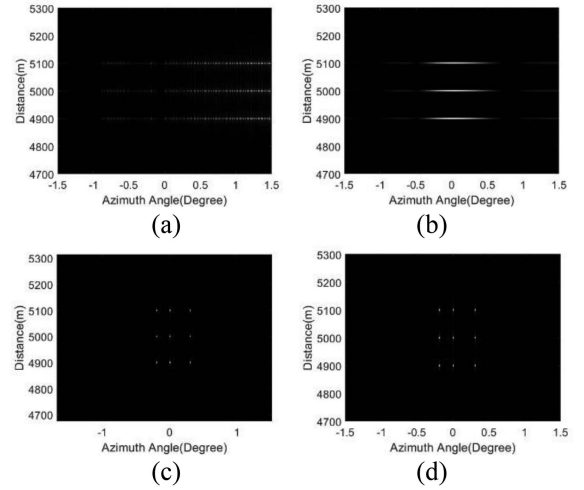

Fig. 5.   Super-resolution results of 2-D array target using different algorithms. (a) IAA. (b) TSVD-L1. (c) TV-L1. (d) Proposed algorithm.
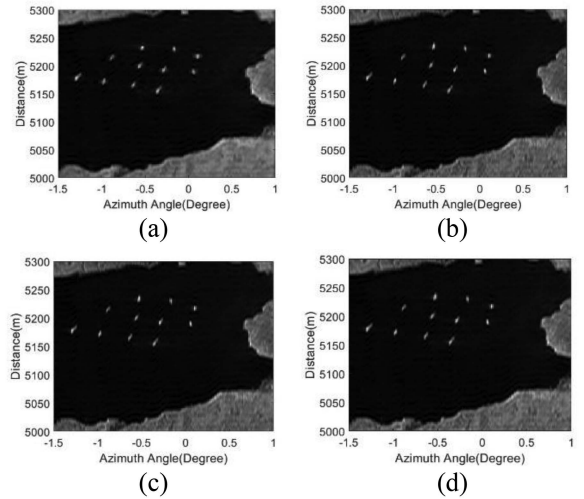

Fig. 6.   Super-resolution results of two-dimensional planar targets using different algorithms. (a) IAA. (b) TSVD-L1. (c) TV-L1. (d) Proposed algorithm.

in the noise, resulting in a failure to achieve the target super-resolution. Although the main information of the target is preserved in the super-resolution result of the TSVD-L1 algorithm, there are still some targets connected together, limiting the resolution. The TV-L1 algorithm can to some extent suppress noise and improve the broadening of the antenna pattern, but there are still some connections that make it difficult to accurately determine the target position and analyze the target. Compared with the aforementioned algorithms under low signal-to-noise ratio conditions, the method proposed in this paper has almost no loss of energy in the recovered target and significantly improves the azimuth resolution.

Fig. 6 shows that both the TSVD-L1 algorithm and the TV-L1 algorithm use L1 norm as a sparse representation in the experiment of recovering frontal targets, which effectively recovers the strong discrete scattering targets at the center of the given frontal targets. The TSVD-L1 algorithm uses the truncated singular
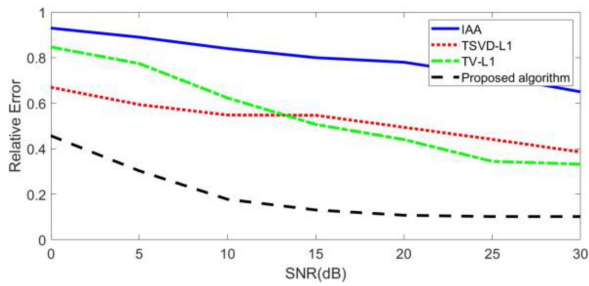
Fig. 7.   Relative error variation curve.

value theory to remove smaller singular values to suppress noise, but due to its inherent algorithmic defects, its resolution is limited. The total variation regularization term in the TV-L1 algorithm ensures a better recovery of contour feature information in the scene. However, the method proposed in this article shows better performance in edge details of the super-resolution results. The strong target points are more prominent and the continuity of the target is better preserved, resulting in a reconstructed image that is closer to the original image.

Comparing the four relative error curves in Fig. 7, even when the signal-to-noise ratio reaches a high 30 dB, the relative error of the IAA algorithm is still above 50%. This is because IAA is essentially a nonparametric weighted least squares algorithm, which is greatly affected by noise and therefore has limited image recovery capability. The performance of the TSVD-L1 algorithm is relatively stable, and it performs the best among the three comparison methods under low signal-to-noise ratio conditions. However, as the signal-to-noise ratio increases, its target recovery performance does not improve significantly. Compared with the TSVD-L1 algorithm, the TV-L1 algorithm has better target recovery performance under high signal-to-noise ratio conditions, but its recovery error is larger under low signal-to-noise ratio conditions. Under all of the signal-to-noise ratio conditions given in this article, the algorithm proposed in this article has smaller relative imaging errors compared to the other three algorithms, and its imaging performance is better.

C. Measured Data Processing

Due to the presence of rich texture information in the target scene, the echo data of the target scene was chosen for the experiment. The antenna scanning speed is 30∘/s, beamwidth is 1.5∘, carrier frequency is 18 GHz, band width is 100 MHz, and PRF is 400 Hz.The red circle in Fig. 8 indicates the echo of the power line in the scene.

Fig. 8(a) shows the real-beam echo image of the scanned radar after pulse compression. In the real-beam echo, the information of some strong scattering points on the upper part of the power line can be vaguely seen, but due to its limited resolution capability, the adjacent strong scattering points on the power lines in the marked area exhibit excessive aliasing in the received echo, and many clutter signals remain around them. As shown in Fig. 8(b)–(d), all three algorithms have a positive effect on the resolution of the power lines. Among them, the TSVD-L1 algorithm has a better recovery effect on the power
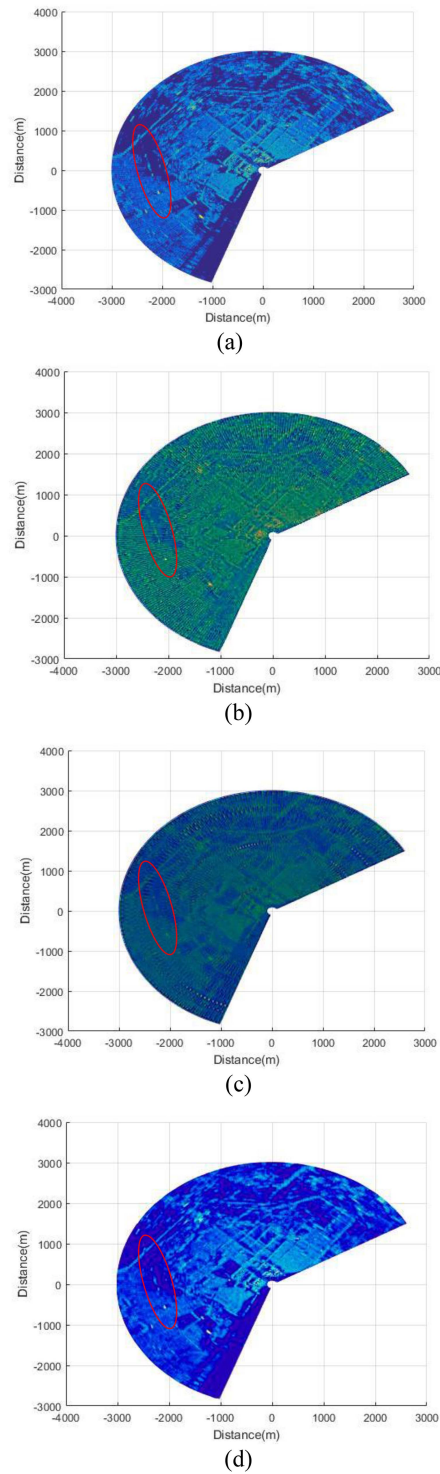

(a)

(b)

(c)

(d)

Fig. 8.   Super-resolution results of measured data in target scenes. (a) Original figure. (b) TSVD-L1. (c) TV-L1. (d) Proposed algorithm.

lines within a small range of high echo intensity, but the recovery results of other parts of the power lines are poor, and the loss of detail information is serious. When the TV-L1 algorithm is used, selecting the total variation operator for solution enhances the recovery of texture contours in the target scene, effectively suppresses interference signals, and achieves better continuity

TABLE IV
ENTROPY OF MEASURED DATA PROCESSING

Method	Entropy
IAA	3.42
TSVD-L1	3.33
TV-L1	3.27
The proposed algorithm	3.18

in the super-resolution imaging results of power lines. When recovering the power lines in the scene using the algorithm proposed in this article, it can be seen that the image quality has been significantly improved, and the texture continuity of the power lines has been well preserved. The method proposed in this article selects the gradient weighting operator of the corresponding power line angle for solution, which weakens the influence of other building lines and more retains the texture characteristics and continuity of power lines. The addition of weight matrix to the error term further enhances the algorithm's ability to suppress noise, and improves the azimuth resolution. In summary, it can be seen from the imaging results that the method proposed in this article has the advantages of both the ITR algorithm and the direction total variation algorithm, and can adjust the adjustable parameters in the Renyi entropy according to different target scenes to achieve optimal imaging performance. To further quantitatively evaluate the results of the different methods, as given in Table IV, the entropy value of the proposed method is lower than the rest of the methods, which further validates the advantages of the proposed method.

V. CONCLUSION

This article proposes an ITR-DTV regularization algorithm based on Renyi entropy. Based on the minimum mean square error as the loss function, the weighted matrix in the ITR algorithm is introduced to more accurately reflect the error level of each measurement value in the loss function. Meanwhile, the DTV operator and Renyi entropy are introduced as regularization items. The experimental results show that compared with other super-resolution imaging methods, the method proposed in this article can more accurately recover the edges and texture details of the image under low signal-to-noise ratio conditions, with richer detail information and stronger adaptability to different target scenes, and has better super-resolution results.

REFERENCES

[1] X. Mengdao et al., "A review of imaging algorithms in multi-platform-borne synthetic aperture radar," *J. Radars*, vol. 8, no. 6, pp. 732–757, 2019.

[2] Y. Zha et al., "Bayesian angular superresolution algorithm for real-aperture imaging in forward-looking radar," *Information*, vol. 6, no. 4, pp. 650–668, 2015.

[3] X. Zhang, M. He, Z. He, H. Su, and J. Zhang, "Research on mono-pulse forward-looking imaging airborne radar system," in *Proc. IET Int. Radar Conf.*, 2013, pp. 1–3.

[4] J. Y. Meng et al., "The lower bound of nonlocal gradient for non-convex and non-smooth image patches based regularization," *Inverse Problems*, vol. 38, no. 3, pp. 1–28, 2022.

[5] M. A. Richards, "Iterative noncoherent angular superresolution (radar)," in *Proc. IEEE Nat. Radar Conf.*, 1988, pp. 100–105.

[6] D. Yiyuan et al., "Improvement of angular resolution of real aperture radar via generalized inverse filtering," *Acta Electronica Sinica*, vol. 1, no. 09, pp. 15–19, 1993.

[7] Y Zha et al., "Bayesian deconvolution for angular super-resolution in forward-looking scanning radar," *Sensors*, vol. 15, no. 3, pp. 6924–6946, 2015.

[8] Z. Liu, X. Y. Tian, and W. Jia, "An image reconstruction algorithm based on Tikhonov regularization in electromagnetic tomography," in *Proc. Int. Conf. Measuring Technol. Mechatron. Automat.*, 2010, pp. 488–491.

[9] J. Hao, G. Chen, Z. Cao, W. Yin, and Q. Zhao, "Image reconstruction algorithm for EMT based on modified Tikhonov regularization method," in *Proc. IEEE Int. Instrum. Meas. Technol. Conf.*, 2012, pp. 2507–2510.

[10] T. Yardibi, J. Li, P. Stoica, M. Xue, and A. B. Baggeroer, "Source localization and sensing: A nonparametric iterative adaptive approach based on weighted least squares," *IEEE Trans. Aerosp. Electron. Syst.*, vol. 46, no. 1, pp. 425–443, Jan. 2010.

[11] Z. Shu, Z. Zong, L. Huang, and L. Huang, "Forward-looking radar super-resolution imaging combined TSVD with l1 norm constraint," in *Proc. IEEE Int. Geosci. Remote Sens. Symp.*, 2019, pp. 2559–2562.

[12] Q. Zhang et al., "TV-sparse super-resolution method for radar forward-looking imaging," *IEEE Trans. Geosci. Remote Sens.*, vol. 58, no. 9, pp. 6534–6549, Sep. 2020.

[13] J. Guan, J. Yang, Y. Huang, and W. Li, "Angular super-resolution algorithm based on maximum entropy for scanning radar imaging," in *Proc. IEEE Geosci. Remote Sens. Symp.*, 2014, pp. 3057–3060.

[14] N. V. Denisova, "Bayesian reconstruction in SPECT with entropy prior and iterative statistical regularization," *IEEE Trans. Nucl. Sci.*, vol. 51, no. 1, pp. 136–141, Feb. 2004.

[15] S. Shlisel and M. Pinchas, "Improved approach for the maximum entropy deconvolution problem," *Entropy (Basel, Switzerland)*, vol. 23, no. 5, pp. 547–547, 2021.

[16] Z X Li and Z L Deng, "A total variation regularization method for an inverse problem of recovering an unknown diffusion coefficient in a parabolic equation," *Inverse Problems Sci. Eng.*, vol. 28, pp. 1453–1473, 2020.

[17] I Bayram and M E Kamasak, "Directional total variation," *IEEE Signal Process. Lett.*, vol. 19, no. 12, pp. 781–784, Dec. 2012, doi: 10.1109/LSP.2012.2220349.

[18] K Bredies, K Kunisch, and T Pock, "Total generalized variation," *SIAM J. Imag. Sci.*, vol. 3, pp. 492–526, 2010.

[19] Y Wang et al., "A new alternating minimization algorithm for total variation image reconstruction," *SIAM J. Imag. Sci.*, vol. 1, no. 3, pp. 248–272, 2008.

[20] S Subramanian and M H Hsieh, "Quantum algorithm for estimating alpha-Renyi entropies of quantum states," *Phys. Rev. A*, vol. 104, no. 2, pp. 1–11, 2021.

[21] H. Liu et al., "An entropy-regularized ADMM for binary quadratic programming," *J. Glob. Optim.*, vol. 87, pp. 447–479, 2023. [Online]. Available: https://doi.org/10.1007/s10898-022-01144-0

[22] W. Li, M. Li, L. Zuo, H. Chen, Y. Wu, and Z. Zhuo, "A computationally efficient airborne forward-looking super-resolution imaging method based on sparse Bayesian learning," *IEEE Trans. Geosci. Remote Sens.*, vol. 61, 2023, Art. no. 5102613, doi: 10.1109/TGRS.2023.3260094.

[23] Y. Zhang et al., "Resolution enhancement for large-scale real beam map based on adaptive low-rank approximation," *IEEE Trans. Geosci. Remote Sens.*, vol. 60, 2022, Art. no. 5116921, doi: 10.1109/TGRS.2022.3202073.

[24] Y. Zhang et al., "High-throughput hyperparameter-free sparse source location for massive TDM-MIMO radar: Algorithm and FPGA implementation," *IEEE Trans. Geosci. Remote Sens.*, vol. 61, 2023, Art. no. 5110014, doi: 10.1109/TGRS.2023.3323517.

Min Bao (Member, IEEE) was born in Kunming, Yunnan Province, China, in 1984. He received the B.S, M.E., and Ph.D. degrees in electronical engineering, circuit and system, and signal and information processing from Xidian University, Xi'an, China, in 2006, 2009, and 2012, respectively.

He is currently an Associate Professor with the School of Electronic Engineering, Xidian University. His research interests include SAR/ISAR applications, through the wall radar.

Zhenhao Jia (Student Member, IEEE) received the B.E. degree in electronic science and technology in 2022 from the School of Optoelectronic Engineering from Xidian University, Shaanxi, China, where he is currently working toward the master's degree in electronic science and technology with the School of Electronic Engineering.

His current research interests include radar forward-looking super-resolution.

Xiaoning Yin (Student Member, IEEE) received the B.E. and the master's degrees in electronic science and technology from the School of Electronic Engineering from Xidian University, Shaanxi, China, in 2019 and 2022, respectively.

Her current research interests include radar forward-looking power line detection.

Mengdao Xing (Fellow, IEEE) received the B.S. degree and Ph.D. degree in signal and information processing from Xidian University, Xi'an, Shaanxi, China, in 1997 and 2002, respectively.

He is currently a Professor with the National Laboratory of Radar Signal Processing, Xidian University. He was the Dean of the Academy of Advanced Interdisciplinary Research Department, Xidian University. He has written or co-written more than 200 refereed scientific journal papers. He also has authored or co-authored two books about SAR signal processing. The total citation times of his research are greater than 10 000 (H-index 50). He was rated as Most Cited Chinese Researchers by Elsevier. He has achieved more than 50 authorized China patents. His current research interests are synthetic aperture radar, SAR interferometry, inversed synthetic aperture radar, sparse signal processing and microwave remote sensing.

Dr. Xing's research has been supported by various funding programs, such as, National Science Fund for Distinguished Young Scholars. He has held several Special Issues on IEEE GRSM and JSTARS. He is currently an Associate Editors for radar remote sensing of IEEE TRANSACTIONS ON GEOSCIENCE AND REMOTE SENSING and the Editor-in-Chief for MDPI Sensors.